Natural Biopolymers: Novel Templates for the Synthesis of Nanostructures

Sonal Padalkar,[†,‡] J. R. Capadona,[§,∥,⊥] S. J. Rowan,[∥,⊥,▽] C. Weder,[#,∥,▽] Yu-Ho Won,[†] Lia A. Stanciu,*[,†,‡] and Robert J. Moon[†,‡,○]

[†]*School of Materials Engineering,* [‡]*Birck Nanotechnology Center, Purdue University, West Lafayette, Indiana 47907,* [§]*Rehabilitation Research and Development, Louis Stokes Cleveland DVA Medical Center, 10701 East Boulevard, Cleveland, Ohio 44106,* [∥]*Department of Macromolecular Science and Engineering,* [⊥]*Department of Biomedical Engineering, and* [▽]*Department of Chemistry, Case Western Reserve University, Cleveland, Ohio 44106,* [#]*Adolphe Merkle Institute and Fribourg Center for Nanomaterials, University of Fribourg, CH-1700 Fribourg, Switzerland, and* [○]*US Forest Service, Forest Products Laboratory, Madison, Wisconsin 53726*

Biological systems such as proteins, viruses, and DNA have been most often reported to be used as templates for the synthesis of functional nanomaterials, but the properties of widely available biopolymers, such as cellulose, have been much less exploited for this purpose. Here, we report for the first time that cellulose nanocrystals (CNC) have the capacity to assist in the synthesis of metallic nanoparticle chains. A cationic surfactant, cetyltrimethylammonium bromide (CTAB), was critical to nanoparticle stabilization and CNC surface modification. Silver, gold, copper, and platinum nanoparticles were synthesized on CNCs, and the nanoparticle density and particle size were controlled by varying the concentration of CTAB, the pH of the salt solution, and the reduction time.

1. Introduction

The synthesis of functional nanomaterials through biomineralization and biotemplating is a topic that is attracting a tremendous amount of interest because of the promise of achieving better control over positioning and connecting different functional nanostructures in complex nanodevices. Starting several years ago, using biomolecular structures such as viruses, proteins, and DNA, the template synthesis of nanomaterials[1−4] has received a tremendous amount of attention in the scientific community. Some biomolecular structures that have been used as biotemplates include microtubules,[5,6] β-amyloid,[7,8] the yeast prion protein Sup35NM,[9] the tobacco mosaic virus,[10] and α-synuclein.[11,12] However, the properties of relatively inexpensive, easily available, and chemically reactive biopolymers have not been fully exploited for the synthesis of inorganic nanoparticles, nanoparticle chains, and nanowires. Polymer nanofibers in general possess specific properties such as high surface area, high chemical or biological reactivity, and in some cases, high porosity. However, taking advantage of these special properties often involves the fabrication of synthetic polymers that could also be both complicated and expensive or involve toxic chemicals and so have similar disadvantages to protein- and DNA-based biomolecular templates. However, natural biopolymer fibers, such as cellulose, are abundant in the biomass and are easily accessible from a range of sources, such as forest products, grasses, tunicates, reeds, and stalks. Cellulose can be a viable alternative to synthetic polymers or even inorganic reinforcing fibers with applications in composite materials.[13−15] Cellulose-based materials are relatively cheap, renewable, abundantly available in a variety of forms, and have hydroxyl groups that are accessible for chemical modification.[16] Previous work includes the synthesis of silver nanoparticles on cellulose acetate nanofibers,[17] the stabilization of gold−silver nanoparticles on cellulose nanocrystals (CNCs),[18] nickel on CNCs,[19] and the deposition of metal nanoparticles into various porous cellulosic matrices.[20−22] Most of these reports show either random deposition into a porous matrix or a rather low coverage of nanoparticles on CNCs. To our knowledge, there are no reports of the synthesis of nanoparticles on the surfaces of tunicate CNCs. The difficulty in applying the same methods for the templated synthesis of nanomaterials on CNC templates that were used by our group and others for the biomineralization of

*Corresponding author. Tel +1-765-496-3552. Fax +1-765- 494-1204. E-mail: lstanciu@purdue.edu.

(1) Cui, Y.; Lieber, C. M. *Science* **2001**, *291*, 851–853.
(2) Duan, X.; Huang, Y.; Cui, Y.; Wang, J.; Lieber, C. M. *Nature* **2001**, *409*, 66–69.
(3) Huang, Y.; Duan, X.; Cui, Y.; Lauhon, L. J.; Kim, K. H.; Lieber, C. M. *Science* **2001**, *294*, 1313–1317.
(4) Duan, X.; Huang, Y.; Agarwal, R.; Lieber, C. M. *Nature* **2003**, *421*, 241–245.
(5) Behrens, S.; Habicht, W.; Wu, J.; Unger, E. *Surf . Interface Anal.* **2006**, *38*, 1014–1018.
(6) Hess, H.; Clemmens, J.; Brunner, C.; Doot, R.; Luna, S.; Ernst, K. H.; Vogel, V. *Nano Lett.* **2005**, *5*, 629–633.
(7) Reches, M.; Gazit, E. *Science* **2003**, *300*, 625–627.
(8) Hamada, D.; Yanagihara, I.; Tsumoto, K. *Trends Biotechnol.* **2004**, *22*, 93–97.
(9) Scheibel, T.; Parthasarathy, R.; Sawicki, G.; Lin, X. M.; Jaeger, H.; Lindquist, S. L. *Proc. Natl. Sci. U.S.A.* **2003**, *100*, 4527–4532.
(10) Flynn, C. E.; Lee, S. W.; Peelle, B. R.; Belcher, A. M. *Acta Mater.* **2003**, *51*, 5867–5880.
(11) Padalkar, S.; Hulleman, J.; Parijat, D.; Kunzeman, K.; Rochet, J. C.; Stach, E. A.; Stanciu, L. *Nanotechnology* **2007**, *18*, 055609/1–055609/9.
(12) Padalkar, S.; Kim, S.-M.; Hulleman, J.; Stach, E. A.; Rochet, J.-C.; Stanciu, L. *Nanotechnology* **2008**, *19*, 275602/1–275602/9.
(13) Capadona, J. R.; Shanmuganathan, K.; Trittschuh, S.; Seidel, S; Rowan, S. J.; Weder, C. *Biomacromolecules* **2009**, *10*, 712–716.
(14) Capadona, J. R.; Shanmuganathan, K.; Tyler, D. K.; Rowan, S. J.; Weder, C. *Science* **2008**, *319*, 1370–1374.
(15) Capadona, J. R.; van den Berg, O.; Capadona, L. A.; Schroeter, M.; Rowan, S. J.; Tyler, D. J.; Weder, C. *Nat. Nanotechnol.* **2007**, *2*, 765–769.
(16) Samir, M. A. S. A.; Alloin, F.; Dufresne, A. *Biomacromolecules* **2005**, *6*, 612–626.
(17) Son, W. K.; Youk, J. H.; Park, W. H. *Carbohydr. Polym.* **2006**, *65*, 430–434.
(18) Shin, Y.; Bae, I. T.; Arey, B. W.; Exarhos, G. J. *J. Phys. Chem. C* **2008**, *112*, 4844–4848.
(19) Shin, Y.; Bae, I. T.; Arey, B. W.; Exarhos, G. J. *Mater. Lett.* **2007**, *61*, 3215–3217.
(20) Cai, J.; Kimura, S.; Wada, M.; Kuga, S. *Biomacromolecules* **2009**, *10*, 87–94.
(21) He, J.; Kunitake, T.; Nakao, A. *Chem. Mater.* **2003**, *15*, 4401–4406.
(22) Maneerung, T.; Tokura, S.; Rujiravanit, R. *Carbohydr. Polym.* **2008**, *72*, 43–51.

proteins, viruses, and DNA results from the CNCs' mostly neutral surface charge (although there are about 85 mmol/kg sulfate groups on the surfaces of these tunicate CNCs). In contrast, proteins or DNA usually display negatively charged groups on their surfaces that can electrostatically interact with metallic cations, which can subsequently be readily reduced to their elemental form.

The current study demonstrates for the first time that by using a modified reductive deposition procedure involving the cationic surfactant cetyltrimethylammonium bromide (CTAB) a reproducible procedure for the metal nanoparticle decoration of tunicate CNCs can be successfully designed.

2. Experimental Section

2.1. Tunicate Cellulose Nanocrystal Processing. Tunicate CNCs were isolated by following a method available in the literature.[23] Briefly, tunicates (Styela Clava) were held at 80 °C for 24 h in an aqueous solution of potassium hydroxide (3 L, 5% w/w per 500 g of tunicate walls) and agitated mechanically. Two more cycles of heating at 80 °C for 24 h at the same concentration as that of the previous solution of KOH were performed. The raw cellulose was washed with water at neutral pH, followed by treatment cycles with 5 mL of acetic acid and 10 mL of hypochlorite solution. Next, the suspension was heated to 60 °C. The acetic acid and hypochlorite treatments were repeated at 1 h intervals until the white color of the cellulose was registered. In the final step, the cellulose was washed with water and transformed into a pulp with a Warring blender. Sulfuric acid hydrolysis of the cellulose pulp was performed to obtain sulfate-functionalized tunicate CNCs. This step was performed in order to achieve a good dispersion of CNCs, and the exact sulfation conditions are available in the original reference.[23]

2.2. Synthesis of Metal Nanoparticles on Cellulose Templates. A multistep process was used to synthesize metallic nanoparticles (Ag, Au, Cu, and Pt) on the surfaces of tunicate CNCs. The same synthesis procedure was used successfully for metal nanoparticle decoration of CNCs in two different types of configurations: (a) CNCs were first deposited onto a carbon-coated copper TEM grid, and the resulting samples were used for TEM analysis. (b) CNCs were first dispersed in DI water brought to an acidic pH (pH 2), and resulting samples were used for UV−vis analysis. The steps in the procedure were (i) 3 μL of a CNC suspension (~2 wt % in DI water at pH ~2) was placed on a TEM grid (for configuration a described above); (ii) 3 μL of CTAB (0.1−1.0 mM) was added to the CNC suspension and allowed to react for 5 min; (iii) 3 μL of the metallic precursor solution (pH 4.5−8.5) was added to the CNC suspension and allowed to react for 5 min; (iv) 3 μL of the reducing agent sodium borohydride ($NaBH_4$) (0.03 wt %) was added to the CNC suspension and held for 5 min; and (v) the substrate was washed with distilled water and dried in air. The synthesis of Ag, Au, Cu, and Pt nanoparticles followed the same procedure with corresponding metal precursors : 0.2 mM to 1 M silver nitrate ($AgNO_3$), 0.8 mM copper chloride ($CuCl_2$), 0.8 mM hydrogen tetrachloroaurate ($HAuCl_4$), and 0.5 mM potassium tetrachloroplatinate (K_2PtCl_4), respectively.

2.3. Characterization of Metallic Nanoparticles. The morphology and size of the nanoparticles deposited on CNC surfaces were characterized by TEM using a Philips CM-10 transmission electron microscope operating at 80 kV. High-resolution transmission electron microscopy (HRTEM) images were obtained to study the crystalline nature of the silver nanoparticles on the CNC. HRTEM images were recorded on an FEI Titan 80/300 transmission electron microscope equipped with a Gatan imaging filter (GIF) and a 2 k CCD operating at 300 kV.

(23) van den Berg, O.; Capadona, J. R.; Weder, C. *Biomacromolecules* **2007**, *8*, 1353–1357.

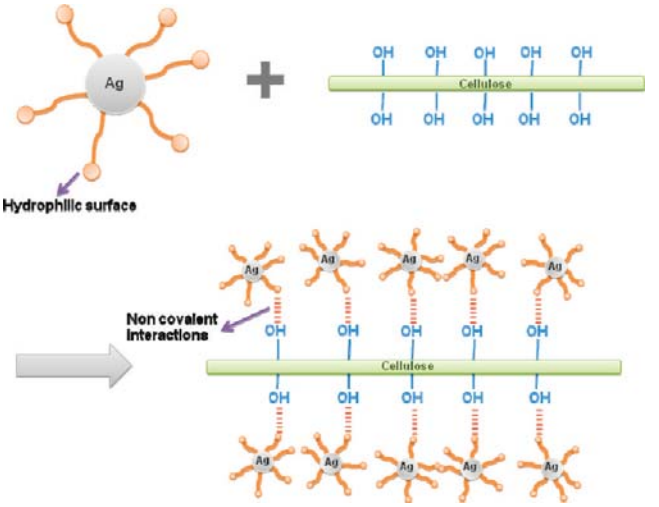

Figure 1. Synthesis mechanism for the formation of Ag nanoparticles on the surfaces of CNCs.

The electron energy loss (EELS) spectrum was obtained to confirm the presence of silver on the cellulose template. The EELS spectrum was also recorded on the FEI Titan. Additionally, a molecular device UV−vis microplate reader was used to measure the UV−vis spectrum of the Ag, Au, Cu, and Pt nanoparticle chains. The metal nanoparticles were synthesized on CNCs in suspension in an Eppendorf tube. The same synthesis procedure outlined in section 2.2 was used, with a CTAB concentration of 0.5 mM. The UV−vis spectrum was obtained after 5 min of reducing time.

3. Results and Discussion

3.1. Role of CTAB in Metal Nanoparticle Synthesis on CNCs. Increasingly, surfactants have been used by chemists and materials scientists as template systems for the stabilization of various types of nanocrystals and nanostructures. CTAB is a cationic surfactant that assembles into micelles in aqueous solution. This surfactant was previously successfully used to stabilize inorganic nanoparticles.[24,25] However, despite a great amount of interest in the scientific community directed toward understanding this micellar system, the exact parameters that control the proven successful stabilization of inorganic nanoparticles[24,25] in the presence of CTAB are still not completely understood. Figure 1 shows our proposed mechanism for the biotemplated synthesis of metallic nanoparticles on the CNC surfaces that are reported in this work. On the basis of previous work that showed that CTAB indeed acts as a stabilizer of inorganic nanoparticles,[24,25] we speculate that Ag nanoparticles are first formed via the conventional reduction of $AgNO_3$ and CTAB acts as a nanoparticle stabilizer. These stabilized nanoparticles, which are covered in polar cationic quaternary ammonium groups, can then noncovalently interact with the polar surfaces of the CNC nanocrystals, which are rich in free hydroxyl groups.

Although the proposed mechanism is not definitive, the theoretical reasoning described above is also supported by the experimental observations that show that for the metal nanoparticle synthesis procedure excluding CTAB there was minimal metal nanoparticle formation on CNCs but extensive formation on the TEM grid substrate (Figure 2a). This is attributed to the fact that cellulose displays mostly neutral hydroxyl groups that do not

(24) Cai, J.; Kimura, S.; Wada, M.; Kuga, S. *Biomacromolecules* **2009**, *10*, 87–94.
(25) Sun, Y.; Yin, Y.; Mayers, B.; Herricks, T.; Xia, Y. *Chem. Mater.* **2002**, *14*, 4736–4745.

interact strongly with the nanoparticles. Note that the sulfate-functionalized tunicate CNCs should have a negative surface charge resulting from the partial sulfonation of the CNCs as a consequence of the sulfuric acid hydrolysis step in the isolation procedure,[26] but it is considered here that the charge density on the CNCs is insufficient to result in a significant formation of metallic nanoparticles on the CNC surface. Figure 2 confirms this point of view by showing that in the absence of CTAB, as a nanoparticle stabilizer and connector to the tunicate nanocrystals, only the nonspecific precipitation of Ag nanoparticles was observed (Figure 2a). After the inclusion of CTAB into the reaction process, Ag nanoparticles are deposited preferentially onto the CNC surfaces (Figure 2b). The Ag particle size was polydisperse and varied between 1 and 20 nm depending on the processing conditions.

The deposition of Ag on CNC surfaces using CTAB was also confirmed for CNCs suspended in DI water (i.e., processing configuration b described in section 2.2). For this case, all of the steps in the Ag nanoparticle synthesis on CNC surfaces were performed in solution. Figure 2c shows that the CNC surface is decorated with Ag particles and therefore the chemical reactions involved in the decoration of CNCs with Ag nanoparticles, in the presence of CTAB, do not need a solid support to occur. Additionally, the depositions of Au, Cu, and Pt on CNC surfaces

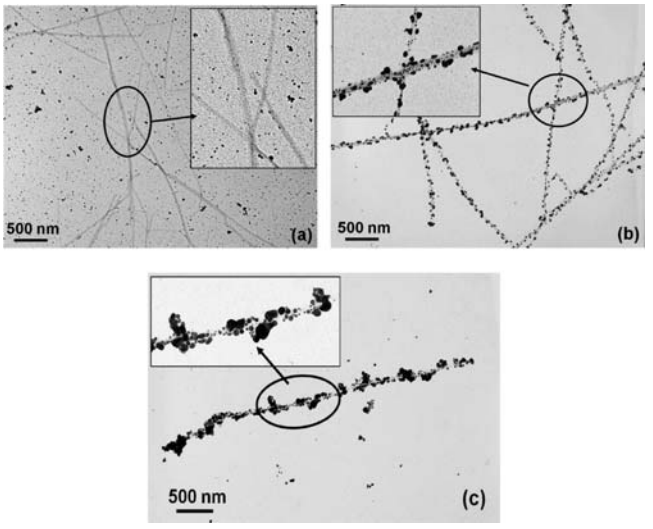

Figure 2. TEM images of Ag nanoparticle synthesis on tunicate CNC: (a) synthesized on a solid support in the absence of CTAB; (b) synthesized on a solid support in the presence of CTAB; and (c) synthesized in the presence of CTAB for CNCs suspended in DI water with no solid support. Regardless of whether the synthesis is performed on a solid support or in solution, when CTAB is used, there is preferential Ag precipitation on CNC rather than on the carbon-coated copper TEM grid substrate.

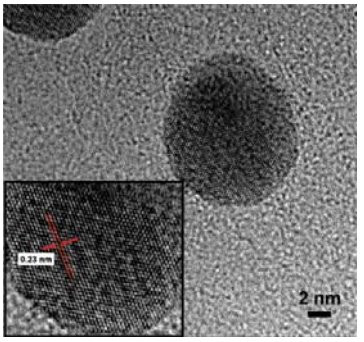

Figure 3. HRTEM image of a single Ag nanoparticle on a CNC. The inset shows the interplannar spacing to be ~0.23 nm, which can be attributed to two (111) planes of Ag.

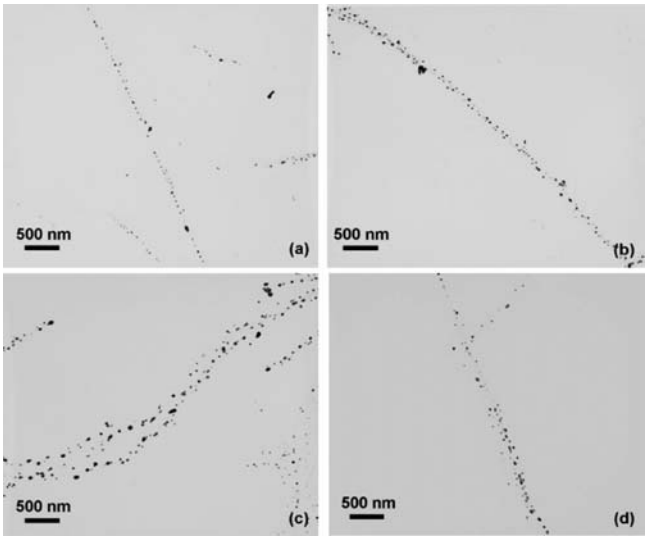

Figure 5. TEM images with varying concentrations of CTAB: (a) 0.1, (b) 0.2, (c) 0.5, and (d) 1.0 mM. These images show that the optimum Ag nanoparticle synthesis on tunicate CNC occurred at 0.5 mM.

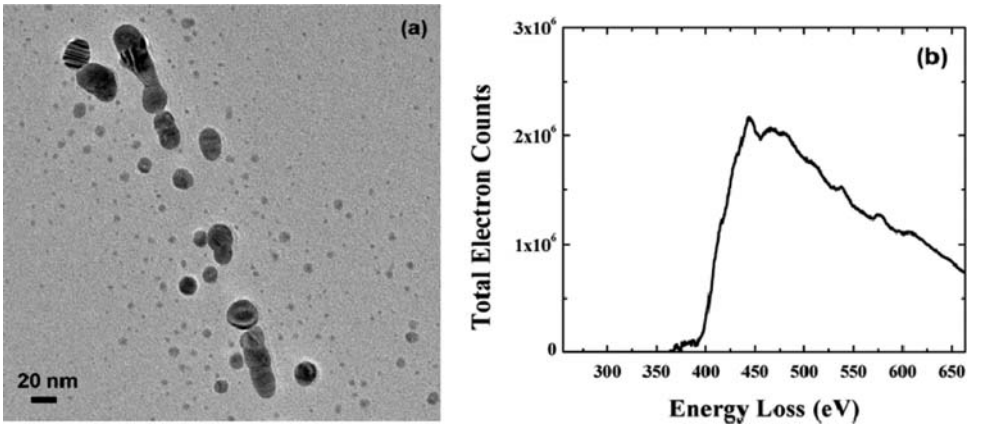

Figure 4. (a) TEM image of an Ag nanoparticle on a CNC surface where an EELS spectrum was obtained. (b) EELS spectrum showing an energy-loss edge at 367 eV.

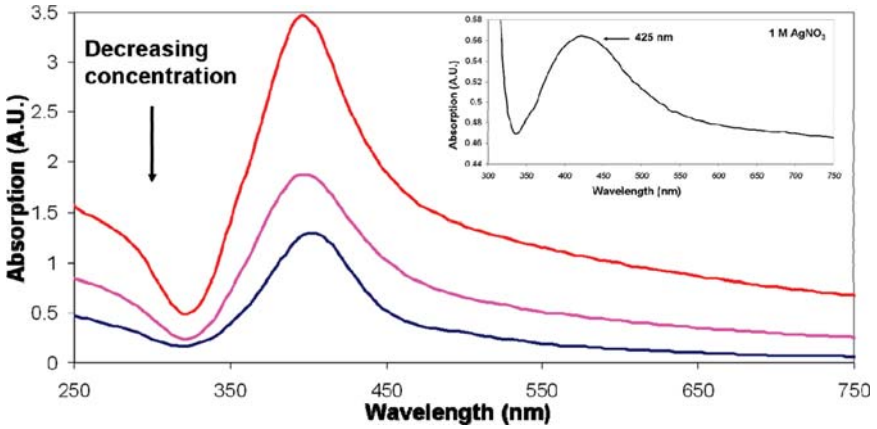

Figure 6. UV−vis absorption spectrum of Ag nanoparticles for 0.2 mM, 10 mM, 100 mM, and 1 M concentrations of $AgNO_3$ salt solution. For 0.2−100 mM concentrations, an absorption peak at ~405 nm was observed whereas for a 1 M concentration an absorption peak was shifted to ~425 nm.

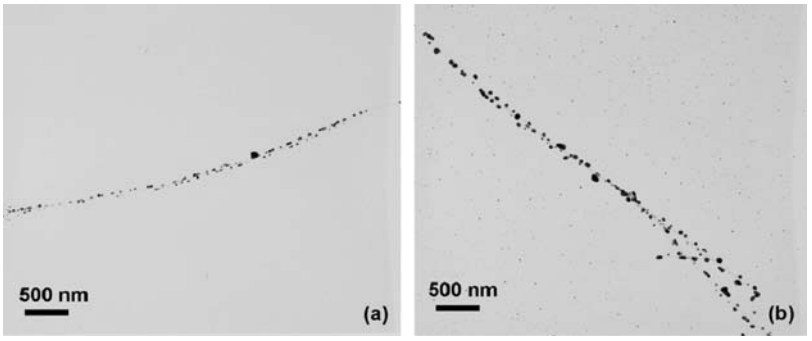

Figure 7. TEM images of Ag nanoparticle samples with varying pH of the $AgNO_3$ salt solution: (a) pH 4.5 and (b) pH 8.5, showing larger Ag particle sizes on the CNCs as well as Ag particle formation on the substrate under the higher-pH condition.

for processing configuration b were also confirmed with subsequent TEM imaging.

3.2. Characterization of Silver Nanoparticles on CNCs. High-resolution transmission electron microscopy (HRTEM) imaging confirmed the presence of faceted Ag nanoparticles on the surfaces of the CNCs. At these extreme magnifications, CNC was not visible because of the low contrast resulting from the lighter elements (C, H, and O) that make up the cellulose as compared to the higher electron density of metallic silver. The HRTEM image (Figure 3) shows lattice fringes of the Ag nanoparticles, indicating their crystallinity, whereas the observation that the entire nanoparticle was not in focus indicates that the Ag nanoparticles were faceted. The Ag nanoparticles imaged for this test had an average size of ~20 nm. The interplanar spacing was measured to be ~0.23 nm and well matched the two (111) planes of Ag (Figure 3 inset). Additionally, EELS further confirmed the formation of Ag on the CNC surface. Figure 4 shows a bright-field TEM image (a) and an EELS spectrum (b) obtained from the same region shown in panel a. The EELS spectrum very clearly shows an Ag major edge at 367 eV, confirming the formation of Ag nanoparticles.

3.3. Optimization of Silver Nanoparticle Formation on CNCs. To obtain an optimum coverage and size distribution of metallic nanoparticles on the CNC surfaces, a study aimed at controlling the fabrication parameters was performed. The first step in this optimization process was to monitor the influence of the concentration of CTAB, followed by the $AgNO_3$ concentration, pH, and reducing time.

3.3.1. CTAB Concentration. The concentration of CTAB was varied from 0.1 to 1.0 mM while keeping the concentration of $AgNO_3$ at 0.2 mM at a pH of 6.5 and a reduction time of 2 min. The nanoparticle coverage increased gradually from 0.1 to 0.5 mM CTAB and then decreased for 1.0 mM CTAB (Figure 5). This is an expected effect that is due to an increase in the number of available micelles for nanoparticle stabilization as the CTAB concentration increases from 0.1 to 0.5 mM. At a CTAB concentration of 1.0 mM, evidence in the literature[27] suggests that the CTAB micelles self-associate into nanorod-like structures and therefore the real concentration of free CTAB micelles available for capping Ag nanoparticles and assembling them on the CNCs is reduced. Noting this, 0.5 mM was considered to be the optimum concentration for nanoparticle synthesis on the cellulose template. All further experiments were performed by keeping the CTAB concentration at 0.5 mM.

3.3.2. $AgNO_3$ Concentration. The concentration of $AgNO_3$ was varied from 0.2 mM to 1 M while the $AgNO_3$ concentration was 0.2 mM at pH 6.5 and an $NaBH_4$ reduction time of 5 min. The effects on Ag nanoparticle formation as a function $AgNO_3$ concentration were measured by UV−vis (Figure 6). The absorption peak centered at ~405 nm corresponds to Ag nanoparticles.[28] The relatively narrow, symmetrical peaks in the UV−vis spectra

(26) Jana, N. R.; Gearheart, L.; Murphy, C. J. *J. Phys. Chem. B* **2001**, *105*, 4065–4070.

(27) Wang, Z.; Liu, J.; Chen, X.; Wan, J.; Qian, Y. *Chem.—Eur. J.* **2005**, *11*, 160–163.

(28) Sun, Y.; Liu, Y.; Zhao, G.; Zhou, X.; Gao, J.; Zhang, Q. *J. Mater. Sci.* **2008**, *43*, 4625–4630.

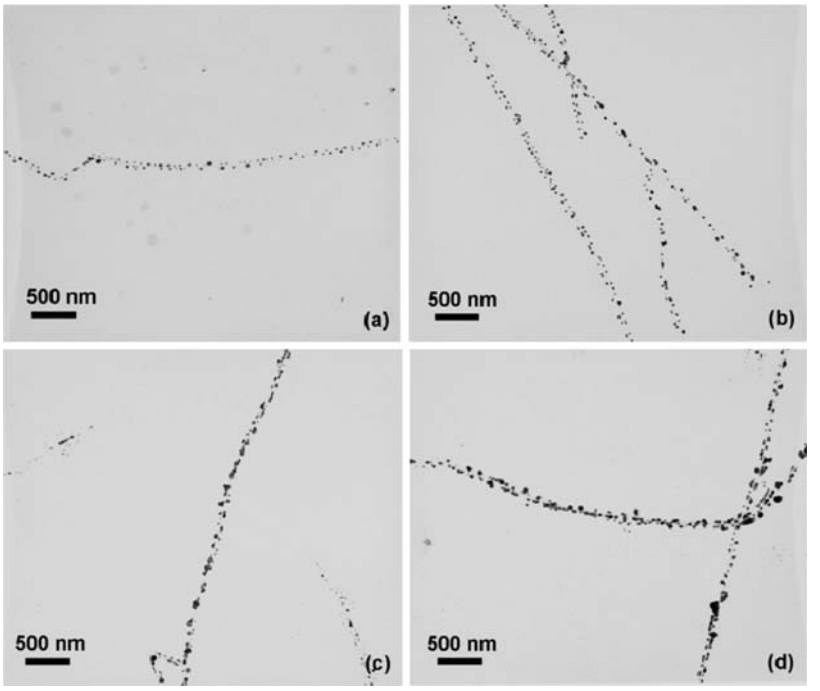

Figure 8. TEM images of Ag nanoparticle with varying $NaBH_4$ reducing times of (a) 2, (b) 5, (c) 15, and (d) 30 min showing a general trend toward larger particle size with increasing reduction time.

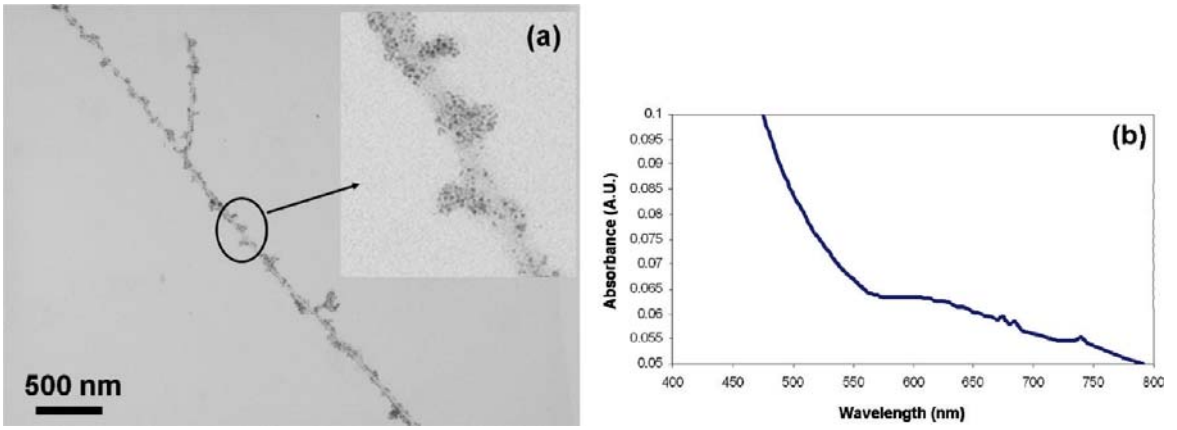

Figure 9. (a) TEM image of Cu nanoparticles on a cellulose template. (b) Absorption spectrum obtained from a Cu sample, showing an absorption peak at ~600 nm.

indicate a narrow Ag particle size distribution. By increasing the $AgNO_3$ concentration from 0.2 mM to 1 M, several observations could be made. The spectra for 0.2, 10, and 100 mM showed an unchanged absorption peak at ~405 nm. With an increase in concentration to above 100 mM, the peaks became broader, indicating a larger particle size distribution. Additionally, for 1 M $AgNO_3$, the UV−vis spectrum appeared to red shift to ~425 nm (Figure 7 inset), which is also considered to be a result of increased Ag particle size.[28] The nucleation of new Ag nanoparticles occurs simultaneously with the growth of other particles. Once the first Ag nuclei are formed, the colliding nuclei start growing while a higher concentration of $AgNO_3$ leads to the formation of new nuclei. This mechanism is also supported by evidence of an increase in the polydispersity of Ag nanoparticles.

3.3.3. pH of $AgNO_3$ Solution. The pH of the $AgNO_3$ salt solution ([$AgNO_3$] = 0.2 mM) was varied between 4.5 and 8.5. The $NaBH_4$ reducing time was kept constant at 5 min. With increased pH, the Ag particle size increased (Figure 7). However, the higher pH values also resulted in a large amount of unspecific silver deposition on the substrate. These results are in agreement with other reports in the literature[28] that indicate that at a basic pH the aggregation of Ag nanoparticles obtained by surfactant stabilization and $NaBH_4$ reduction occurs. This effect can be attributed to hydrophobic interactions between uncharged CTAB molecules at slightly basic pH, rendering them insoluble (i.e., unable to stabilize and prevent Ag nanoparticle aggregation).

3.3.4. $NaBH_4$ Reducing Time. The $NaBH_4$ reducing time was varied from 2 to 30 min. The pH of the $AgNO_3$ salt solution was 6.5, and the concentration was 0.2 mM. The effect on Ag particle formation and size was analyzed by TEM (Figure 8). With increased reaction time, the average Ag particle size increased from ~17 to ~36 nm.

3.4. Synthesis of Copper, Gold, and Platinum Nanoparticles on CNCs. To investigate the capacity of the CNC template synthesis platform to be extended to other inorganic nanoparticle

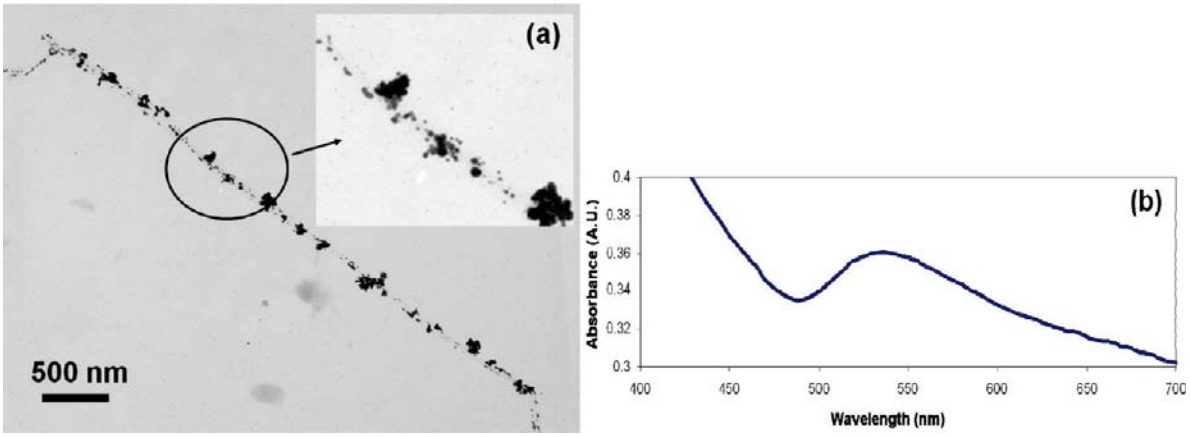

Figure 10. (a) TEM image of Au nanoparticles on a cellulose template. (b) Absorption spectrum obtained from an Au sample, showing an absorption peak at ~535 nm.

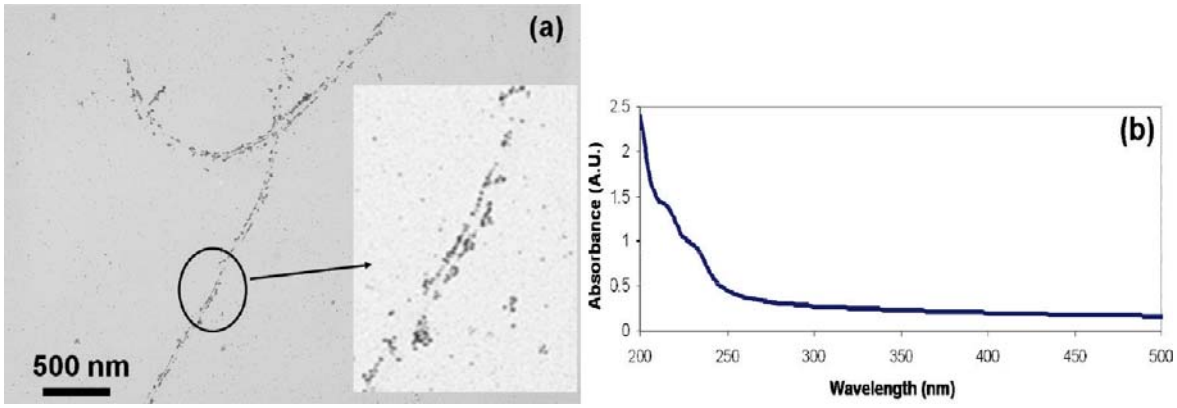

Figure 11. (a) TEM image of Pt nanoparticles on a cellulose template. (b) Absorption spectrum obtained from a Pt sample, showing an absorption peak in the range of ~210−300 nm.

syntheses, metallic nanoparticles of Cu, Au, and Pt were also fabricated on CNC surfaces by the general procedure described in section 2.2 (pH 4.5, [CTAB] = 0.5 mM, 5 min of reduction time) and were then characterized by TEM and UV−vis. The morphology of these metallic nanoparticles was similar to that of Ag nanoparticles. Figure 9a shows a bright-field TEM image of the Cu nanoparticle sample. The average size of Cu nanoparticles was ~5 nm, and the particles appeared to have agglomerated on the CNC surface. The UV−vis absorption peak at ~600 nm indicates the formation of Cu nanoparticles.[29,30] For the Au synthesis, the nanoparticles appear to be agglomerated, have a wider range of size (5−20 nm), and form several large gaps along the CNC (Figure 10). The UV−vis absorption peak at ~535 nm indicates the formation of Au nanoparticles.[31,32] In contrast, for the Pt synthesis, the average size of the nanoparticles was ~5 nm and the particles were relatively uniformly distributed along the CNC length (Figure 11). The UV−vis spectrum peak is in the range of ~200−300 nm, indicating the formation of platinum nanoparticles.[33,34]

4. Conclusions

The surfaces of tunicate CNCs were decorated along their length with metallic nanoparticles. For the first time, a cationic surfactant (CTAB) was used, not only as a stabilizer of metallic nanoparticles but also as a vehicle for the positioning of these particles on the CNCs surface. This method resulted in the successful decoration of CNC surfaces with Ag, Cu, Au, and Pt nanoparticles. The nanoparticles were polydisperse, which was believed to result from the competing nucleation and growth mechanism that dominates their formation. The average size of the nanoparticles and coverage on the CNC were controlled by varying the concentration of the surfactant, the salt solution, the reaction time, and the pH of the salt solution.

Acknowledgment. We thank the U.S. Forest Service for funding this project.

(29) Dhas, N.; Raj, C.; Gedanken, A. *Chem. Mater.* **1998**, *10*, 1446–1452.
(30) Creighton, J.; Eadon, D. *J. Chem. Soc., Faraday Trans.* **1991**, *87*, 3881.
(31) Hu, X.; Zhao, Q.; Jiang, X.; Zhu, C.; Qiu, J. *Solid State Commun.* **2006**, *138*, 43–46.
(32) Zheng, J.; Zhang, C.; Dickson, R. *Phys. Rev. Lett.* **2004**, *93*, 077402–1.
(33) Kim, A.; Bae, D.; Shin, H.; Hong, K. *J. Phys.: Condens. Matter* **2004**, *16*, 3199–3206.
(34) Ershov, B.; Sukhov, N. *Russ. J. Phys. Chem.* **2001**, *75*, 130.